

Electron-Transfer Studies of a Peroxide Dianion

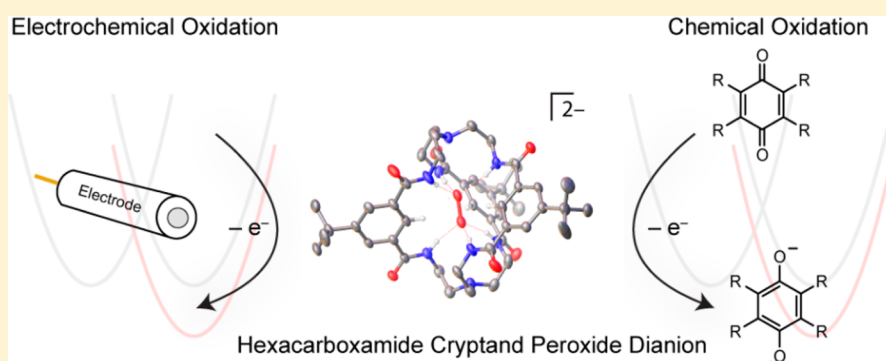
Andrew M. Ullman,[†] Xianru Sun,[‡] Daniel J. Graham,[†] Nazario Lopez,[§] Matthew Nava,[§] Rebecca De Las Cuevas,[§] Peter Müller,[§] Elena V. Rybak-Akimova,[‡] Christopher C. Cummins,^{*,§} and Daniel G. Nocera^{*,†}

[†]Department of Chemistry and Chemical Biology, Harvard University, 12 Oxford Street, Cambridge, Massachusetts 02138, United States

[§]Department of Chemistry, Massachusetts Institute of Technology, 77 Massachusetts Avenue, Cambridge, Massachusetts 02139, United States

[‡]Department of Chemistry, Tufts University, 62 Talbot Avenue, Medford, Massachusetts 02155, United States

S Supporting Information



ABSTRACT: A peroxide dianion (O_2^{2-}) can be isolated within the cavity of hexacarboxamide cryptand, $[(\text{O}_2)\text{CmBDCA-5t-H}_6]^{2-}$, stabilized by hydrogen bonding but otherwise free of proton or metal-ion association. This feature has allowed the electron-transfer (ET) kinetics of isolated peroxide to be examined chemically and electrochemically. The ET of $[(\text{O}_2)\text{CmBDCA-5t-H}_6]^{2-}$ with a series of seven quinones, with reduction potentials spanning 1 V, has been examined by stopped-flow spectroscopy. The kinetics of the homogeneous ET reaction has been correlated to heterogeneous ET kinetics as measured electrochemically to provide a unified description of ET between the Butler–Volmer and Marcus models. The chemical and electrochemical oxidation kinetics together indicate that the oxidative ET of O_2^{2-} occurs by an outer-sphere mechanism that exhibits significant nonadiabatic character, suggesting that the highest occupied molecular orbital of O_2^{2-} within the cryptand is sterically shielded from the oxidizing species. An understanding of the ET chemistry of a free peroxide dianion will be useful in studies of metal–air batteries and the use of $[(\text{O}_2)\text{CmBDCA-5t-H}_6]^{2-}$ as a chemical reagent.

INTRODUCTION

Aerobic life is driven by the thermodynamic potential provided by dioxygen (O_2). In its ground state, O_2 is kinetically stable with respect to the chemical bonds found in living organisms. The controlled activation of O_2 in nature is therefore mediated by electron transfer (ET) to produce its diatomic congeners of superoxide ($\text{O}_2^{\bullet-}$) and peroxide (O_2^{2-}).¹ In nonaqueous environments, superoxide is stable in the absence of electrophilic species such as protons or metal ions, and the anion exhibits reversible ET behavior; accordingly, the outer-sphere oxidation of superoxide has been comprehensively studied using chemical and electrochemical techniques.^{2–4} The ET chemistry of peroxide as an isolated species, however, remains ill-defined because the dianion is not readily available in free form. Peroxide is extremely unstable under nonaqueous conditions because of its ability to act as a strong Brønsted base.⁵ For example, the electrochemical reduction of superoxide

at a gold electrode in dimethyl sulfoxide (DMSO), and in the presence of tetraethylammonium (TEA) perchlorate, results in deprotonation-induced decomposition of the TEA cation to form protonated peroxide (HO_2^-), which in turn, oxidizes DMSO to dimethyl sulfone (DMSO_2).⁶ Peroxide is therefore stabilized by coordination to a metal ion, and hence the intrinsic oxidation–reduction properties of the isolated dianion are difficult to establish because of metal–oxygen orbital mixing and electrostatic effects. Given the importance of peroxide as a deleterious intermediate in the biochemical reduction of molecular O_2 ,⁷ as a valuable industrial feedstock,⁸ and, in particular, as a primary discharge product in nonaqueous lithium–air batteries,^{9,10} it is desirable to understand the basic

Received: April 5, 2014

Published: April 28, 2014

ET properties of peroxide uncoupled from the complicating effects of protons or metal ions.

We have discovered that a soluble source of discrete O_2^{2-} units can be isolated by using hexacarboxamide cryptand (*m*BDCA-5t- H_6) as a sequestering agent (Figure 1).¹¹ The

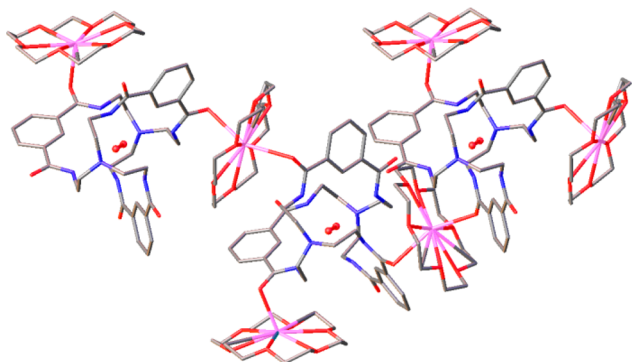


Figure 1. View of the crystal structure of $[K(18\text{-crown-}6)]_2[(O_2)CmBDCA\text{-}5t\text{-}H_6]$ depicting the 1D coordination polymer formed in the solid state. Solvents of crystallization, *tert*-butyl groups, and hydrogen atoms are omitted for clarity. Color code: C, gray; N, blue; O, red; K, pink.

dianion does not interact with surrounding cations, and O_2 is released upon chemical oxidation of the sequestered dianion. This simple oxidative ET serves as a model for the desired half-reaction needed for a rechargeable lithium–air battery, for which a large overpotential is required. This overpotential has been the subject of numerous studies^{12–14} and remains a hurdle in the pursuit of a practical metal–air battery.¹⁵ Herein, we report the ET kinetics of chemical and electrochemical oxidation of $[(O_2)CmBDCA\text{-}5t\text{-}H_6]^{2-}$, with the goal of providing insight into the inherent properties germane to peroxide oxidation. Knowledge of the ET behavior from discrete O_2^{2-} is useful not only for the design of metal–air batteries capable of recharging at lower overpotentials but also for the informed use of a cryptand-encapsulated O_2^{2-} oxidant and/or atom-transfer reagent, in chemical transformations.

EXPERIMENTAL SECTION

General Methods. All manipulations were performed either with use of Schlenk techniques or in a nitrogen-atmosphere glovebox. All reagents were purchased from Aldrich. Quinones were sublimed three times. Solvents (EMD Chemicals) were either used as received or purified on a Glass Contour Solvent Purification System built by SG Water USA, LLC. IR spectra were recorded on a Bruker Tensor 37 Fourier transform infrared (FTIR) spectrometer. NMR solvents were obtained from Cambridge Isotope Laboratories, and 1H and $^{13}C\{^1H\}$ NMR spectra were obtained on a Varian 300 MHz or a Bruker 400 MHz spectrometer and are referenced to residual solvent signals. Elemental analyses were performed by Midwest Microlabs, LLC.

Crystallography. Low-temperature diffraction data were collected on a three-circle diffractometer coupled to a Bruker-AXS Smart Apex charged-coupled-device (CCD) detector with graphite-monochromated Mo $K\alpha$ radiation ($\lambda = 0.71073 \text{ \AA}$) for the structure of $[K(18\text{-crown-}6)]_2[(O_2)CmBDCA\text{-}5t\text{-}H_6]$, performing φ and ω scans. The structures were solved by direct methods using *SHELXS* and refined against F^2 on all data by full-matrix least squares with *SHELXL-97* using established methods.¹⁶ All non-hydrogen atoms were refined anisotropically.¹⁷

Preparative Methods. For $[K(18\text{-crown-}6)]_2[(O_2)CmBDCA\text{-}5t\text{-}H_6]$, *m*BDCA-5t- H_6 (0.587 mmol, 1.00 equiv), 18-crown-6 (1.292 mmol, 2.2 equiv), and KO_2 (1.292 mmol, 2.2 equiv) were loaded into

a 100 mL Schlenk flask and 30 mL of dry tetrahydrofuran (THF) was added. This reaction mixture was stirred under N_2 with the vessel connected to the Schlenk line. The contents formed a white-yellow slurry. A yellow solution was formed after 12 h. This reaction mixture was stirred for 24 h with no evident color change. The contents were subjected to three cycles of freeze–pump–thaw and brought into the glovebox. The remaining insoluble materials were removed by filtration, and the solid was washed with $3 \times 5 \text{ mL}$ of THF to dissolve any peroxide adduct that might have precipitated. THF was removed under a dynamic vacuum. The contents were redissolved in a minimum amount of THF (10 mL). The product was induced to precipitate by adding Et_2O dropwise with stirring. Excess 18-crown-6 was removed by washing the yellow solid with $3 \times 10 \text{ mL}$ of Et_2O . A sample of the yellow solid was dissolved in $DMSO\text{-}d_6$, and a 1H NMR spectrum was taken. The 1H NMR spectrum indicated complete conversion to the peroxide adduct. Single crystals were obtained after 4 days by vapor diffusion of diethyl ether into a THF solution of $[K(18\text{-crown-}6)]_2[(O_2)CmBDCA\text{-}5t\text{-}H_6]$. Yield: 0.80 g (0.54 mmol, 91%). ATR-FTIR on solid: (N–H) 3272 cm^{-1} . 1H NMR (300 MHz, $DMSO\text{-}d_6$, δ): 14.63 (s, 6 H), 10.10 (s, 3 H), 8.16 (s, 6 H), 3.53 (s, 48 H), 3.39 (br, 6 H), 2.60 (br d, 6 H), 2.33 (br d, 12 H), 1.32 (s, 27 H). NMR (100 MHz, $DMSO\text{-}d_6$, δ): 165.56, 148.90, 134.99, 126.70, 124.23, 69.39, 59.97, 40.79, 34.40, 31.19. Anal. Calcd (found) for $C_{72}H_{114}N_8O_{20}K_2$: C, 58.04 (57.90); H, 7.71 (7.72); N, 7.52 (7.44).

Stopped-Flow Kinetic Measurements. THF solutions of the reagents were prepared in an MBraun glovebox filled with ultrahigh-purity argon (Airgas) and placed in Hamilton gastight syringes equipped with three-way valves. Time-resolved spectra (380–800 nm) were acquired over a range of temperatures using a Hi-Tech Scientific KinetAsyst SF-61DX2 Multi-Mixing CryoStopped-Flow system (TgK Scientific Ltd.) equipped with a quartz tungsten halogen light source, a J&M TIDAS diode-array detector, and a Brandenburg 4479 series PMT monochromator. The instrument was equipped with poly(ether ether ketone) tubing fitted inside stainless steel plumbing, a 1.00 cm^3 quartz mixing cell submerged in an ethanol cooling bath, and an anaerobic kit purged with argon. The temperature in the mixing cell was maintained to $\pm 0.1 \text{ }^\circ\text{C}$, and the mixing time was 2–3 ms. All flow lines of the instrument were extensively washed with degassed, anhydrous THF before charging the driving syringes with reactant solutions. The reactions were studied by rapid-scanning spectrophotometry under second-order conditions with a 1:1 molar ratio of the two reactants. All of the experiments were performed in a single-mixing mode of the instrument, with a 1:1 (v/v) mixing ratio. A series of three or four measurements gave an acceptable standard deviation (within 10%). Data analysis was performed with Kinetic Studio (TgK Scientific Ltd.) and IGOR Pro 5.0 (Wavemetrics, Inc.).

Electrochemical Methods. Cyclic voltammograms (CVs) were collected using a CH Instruments (Austin, TX) 730C potentiostat. Solutions of 0.5 mM $[TBA]_2[(O_2)CmBDCA\text{-}5t\text{-}H_6]$ in *N,N*-dimethylformamide (DMF; 0.1 M $[TBA][PF_6]$) were prepared in a nitrogen glovebox. The cell was covered with a Teflon cap containing the electrodes and sealed with parafilm. It was then removed from the glovebox and immediately placed under a blanket of argon. The temperature was controlled by placing the cell in an ethylene glycol bath kept at 298 K. The working electrode was freshly polished glassy carbon (area = 0.07 cm^2), the counter electrode was a platinum wire, and a fresh silver wire in DMF (0.1 M $[TBA][PF_6]$) separated from the working solution by a vycor frit was used as a pseudoreference electrode. Prior to use, DMF had been dried by passage through an alumina column followed by exposure to activated 4 Å sieves overnight. At the conclusion of the experiments, ferrocene was added and all potentials were referenced to the ferrocenium/ferrocene ($Fc^{+/0}$) couple.

Electrochemical Modeling. The diffusion coefficient (D) and reduction potential (E_0) of O_2 were determined from a CV of a 4.6 mM (saturated) solution of O_2 in DMF (0.1 M $[TBA][PF_6]$). The diffusion coefficient of $O_2^{\bullet-}$ was approximated as $1/3 D(O_2)$.¹⁸ The literature value for the heterogeneous rate constant (k_s) of 0.093 cm/s O_2 in DMSO (0.1 M $[TBA][ClO_4]$) was used.¹⁹ All other quantities

were varied in the *DigiElch* software suite²¹ until a satisfactory fit to the experimental data was achieved with reasonable values.

RESULTS

Synthesis. The sequestration of K^+ ions of $[K_2(DMF)_5] \cdot [(O_2)CmBDCA-St-H_6]$ by 18-crown-6 affords the appropriation of $[K(18-crown-6)]_2[(O_2)CmBDCA-St-H_6]$ in 73% isolated yield and engenders good solubility of the complex in THF.¹¹ Alternatively, a more facile preparative route of $[K(18-crown-6)]_2[(O_2)CmBDCA-St-H_6]$ was found, which avoids the extra step of isolating $[K_2(DMF)_5] \cdot [(O_2)CmBDCA-St-H_6]$. For this method, a slurry of $mBDCA-St-H_6$ and 2.2 equiv of 18-crown-6 is treated with 2.2 equiv of KO_2 in THF, resulting in a 91% isolated yield for the peroxide-guest complex. The 1H NMR spectra of compounds obtained by either of these preparative methods are identical except for the additional resonances corresponding to 18-crown-6 (Figure S1 in the Supporting Information, SI). Single crystals of the complex were obtained by vapor diffusion of Et_2O into a THF solution of $[K(18-crown-6)]_2[mBDCA-St-H_6]$. The solid-state structure reveals two environments for the K^+ ions: one ion is coordinated to the CO of neighboring cryptands, forming a 1D coordination polymer, and the other one is bound terminally (Figure 1).

Electrochemical Oxidation. CVs of $[TBA]_2[(O_2)CmBDCA-St-H_6]$ under an atmosphere of argon exhibit oxidation and reduction features (Figure 2). The

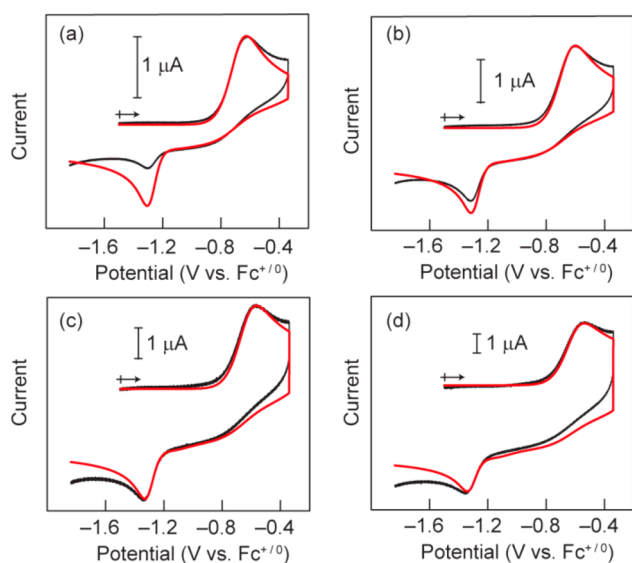


Figure 2. Experimental (black solid line) and simulated (red solid line) CVs of 0.5 mM $[TBA]_2[(O_2)CmBDCA-St-H_6]$ in DMF (0.1 M $[TBA][PF_6]$) at (a) 50, (b) 100, (c) 250, and (d) 500 mV/s. Crosses and arrows depict the initial point and direction of the scan.

reduction wave, which we have attributed to the chemically irreversible reduction of O_2 , only appears after oxidation of $[(O_2)CmBDCA-St-H_6]^{2-}$ (Figures S2 and S3 in the SI).¹¹ The oxidation peak current (i_p) displayed a linear variation with the square root of the scan rate (ν ; Figure S4 in the SI), indicating well-defined Cottrell kinetics for a soluble diffusion-controlled species. The oxidation peak potential (E_p) varied linearly with $\log(\nu)$ with a slope equal to 95 mV/decade (Figure S5 in the SI), which is inconsistent with an electrochemically reversible ET or an ET followed by a chemical step (30 mV/decade)

according to Butler–Volmer kinetics for $\alpha = 0.5$.²⁰ This result, together with the broadness of the oxidation wave, indicates that ET attendant to the cryptand peroxide oxidation process is not an electrochemically or chemically facile process.

The broad oxidation wave may be modeled according to the Butler–Volmer formalism using $\alpha = 0.38$ for the one-electron oxidation of $[TBA]_2[(O_2)CmBDCA-St-H_6]$.¹¹ The data can also be described using the Marcus–Hush model of electrode kinetics. Figure 2 shows that a satisfactory representation of the data is achieved for all scan rates using electrochemical simulation software, such as *DigiElch*,²¹ with a reorganization energy $\lambda = 0.79$ eV, an ET rate constant of $k_s = 2.7 \times 10^{-5}$ cm/s, and a standard reduction potential of $O_2^{\bullet-}/O_2^{2-}$ within the cryptand of -0.85 V versus $Fc^{+/0}$ (Table S1a,b in the SI). The poor fit at low scan rates of the reduction of free O_2 is ascribed to unwanted convection contributions to the current.

Chemical Oxidation with Quinones. Quinones are rapidly reduced by $[(O_2)CmBDCA-St-H_6]^{2-}$, requiring the use of stopped-flow spectroscopy at low temperature in order to determine the ET reaction rate. Dichlorodicyanoquinone (DDQ) cleanly reacts with $[K_2(DMF)_5] \cdot [(O_2)CmBDCA-St-H_6]$ in DMF under stoichiometric conditions to produce free O_2 (quantified by gas chromatography), free cryptand, and the DDQ dianion, DDQ^{2-} .¹¹ However, DMF could not be used as a solvent in the stopped-flow measurements because of the solvent's relatively high freezing point, relatively high viscosity, and incompatibility with some materials used to seal the flow lines of the instrument. Thus, THF was employed instead, necessitating the use of the more soluble $[K(18-crown-6)]_2[(O_2)CmBDCA-St-H_6]$ complex.

The kinetics of the reaction between $[K(18-crown-6)]_2[(O_2)CmBDCA-St-H_6]$ and DDQ was measured over a broad temperature range (-85 to $+25$ °C) under second-order conditions with equal concentrations of reactants. Reaction times varied when the stopped-flow experiment was performed in the diode-array mode as opposed to reproducible reaction times when the experiment was performed in the single-wavelength mode. Intense illumination with white light was used in the former case, whereas low-intensity, monochromatic visible light was used in the latter. These effects indicate photosensitivity of the reaction, which is circumvented in single-wavelength-mode detection. Thus, only single-wavelength data measured at $\lambda = 601$ nm was used for kinetic analyses.

Figure 3a shows the time-resolved visible absorption trace of the formation of a species at low temperature (-85 °C) with absorption maxima at $\lambda = 445$, 561, and 601 nm. These features are consistent with $DDQ^{\bullet-}$,²² which forms rapidly. The kinetics for the prompt appearance of $DDQ^{\bullet-}$ is in accordance with the ET reaction



where $L = mBDCA-St-H_6$. The initial rate of formation of the anion (inset in Figure 3a) fits pseudo-first-order reaction kinetics,

$$\text{rate} = ae^{-k_{\text{obs}}t} \quad (2)$$

to yield the observed rate constants k_{obs} (Figure S6 in the SI), from which second-order ET rate constants k_{ET} were estimated using $k_{\text{ET}} = k_{\text{obs}}/[DDQ] = 4 \times 10^6 \text{ M}^{-1} \text{ s}^{-1}$. No pronounced differences in the values of k_{ET} were found at the three temperatures studied (Table S2 in the SI), which is likely due

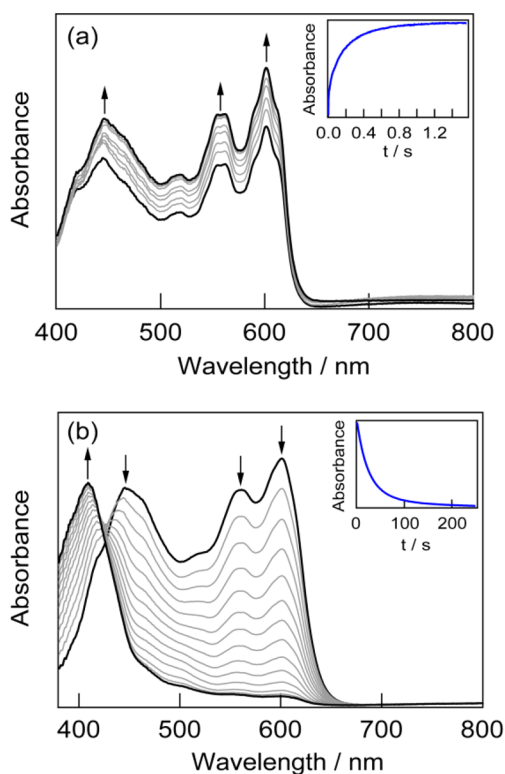
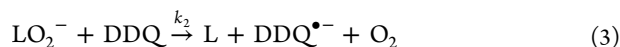


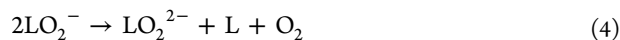
Figure 3. (a) Time-resolved spectral changes obtained upon mixing THF solutions of $[K(18\text{-crown-6})]_2[(O_2)CmBDCA\text{-}5t\text{-}H_6]$ (0.05 mM) and DDQ (0.05 mM) at $-85\text{ }^\circ\text{C}$, showing rapid formation of the $DDQ^{\bullet-}$ radical anion. (b) Time-resolved spectral changes obtained upon mixing THF solutions of $[K(18\text{-crown-6})]_2[(O_2)CmBDCA\text{-}5t\text{-}H_6]$ (0.1 mM) and DDQ (0.1 mM) at $20\text{ }^\circ\text{C}$. The insets are the kinetic traces at $\lambda = 601\text{ nm}$. All concentrations are reported after mixing in the stopped-flow cell.

to our inability to accurately observe a difference in the rate with sufficient fidelity over this small temperature range. Accordingly, accurate activation parameters could not be obtained.

After the initial absorption rapidly increased because of the formation of $DDQ^{\bullet-}$, more quinone anion appeared in two slower steps (Figures S7 and S8 in the SI). The formation of the quinone monoanion on slower time scales is consistent with the bimolecular reaction of the superoxide cryptand complex produced from reaction (1)



or from the disproportionation reaction of the superoxide adduct



followed by the reaction of LO_2^{2-} with DDQ per reaction (1). Superoxide in the presence of free cryptand rapidly produces LO_2^{2-} and O_2 . Hence, we believe that superoxide disproportionation is facile and that one of the slower events that leads to $DDQ^{\bullet-}$ is most likely due to reaction (4), followed by reaction (1). This slower growth of $DDQ^{\bullet-}$ appeared to be complete within tens of seconds (Figure S7 in the SI). Because the time scale for this event was well separated from the initial kinetic phase, the slow process could be examined independently from reaction (1) over a broad temperature range (-85 to $-59\text{ }^\circ\text{C}$). Activation parameters for this event are extracted from the data

presented in Figure S9 in the SI and are summarized in Table S2 in the SI. Monitoring the reaction for several minutes at low temperature (see Figure S8 in the SI) revealed yet an additional, though minor, absorption growth phase. Because these secondary growth phases associated with reactions (3) and (4) were slow with respect to the kinetics of reaction (1), they posed no interference to analysis of the ET kinetics of peroxide as described by reaction (1).

Whereas $DDQ^{\bullet-}$ persists at low temperature, it disproportionates to DDQ and DDQ^{2-} at higher temperatures, as evidenced by growth of the dianion's characteristic spectral features, the most prominent of which is a band at $\lambda_{\text{max}} \sim 417\text{ nm}$.²² Figure 3b shows this conversion at $20\text{ }^\circ\text{C}$. Figure S10 in the SI presents the time-dependent bleach at $\lambda = 601\text{ nm}$ that accompanies this transformation at $5\text{ }^\circ\text{C}$. Formation of DDQ^{2-} may occur by either the reaction of $DDQ^{\bullet-}$ with the cryptand superoxide or cryptand peroxide complex. The activation parameters for the appearance of DDQ^{2-} are derived from the kinetic data in Figure S11 in the SI, and they are summarized in Table S2 in the SI. Because conversion of DDQ^- to DDQ^{2-} occurs over long time scales and only at higher temperature, this process does not interfere with examination of the ET kinetics of reaction (1).

To further elucidate the ET chemistry of the LO_2^{2-} adduct, the ET reactions of six additional quinones (Br_4Q , Cl_4Q , F_4Q , Cl_2Q , ClQ , and H_4Q ; see Table 1) were examined by the stopped-flow method. The overall driving force of the reaction

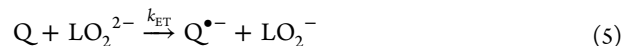


Table 1. Driving-Force and ET Rate Constants of Quinone/ LO_2^{2-} at $-80\text{ }^\circ\text{C}$ for Reaction (5)

Quinone	E_{red}^a	ΔG° (V)	k_{ET} ($M^{-1}\text{ s}^{-1}$) ^b
DDQ	0.13	-0.98	$3.83(27) \times 10^6$
Cl_4Q	-0.37	-0.48	$3.03(8) \times 10^6$
Br_4Q	-0.38	-0.47	$7.98(84) \times 10^5$
F_4Q	-0.42	-0.43	$2.35(22) \times 10^6$
Cl_2Q	-0.56	-0.29	$1.67(11) \times 10^4$
ClQ	-0.72	-0.13	$3.20(24) \times 10^2$
H_4Q	-0.89	0.04	2.57^c

^aReduction potentials of quinones are referenced versus $Fc^{+/0}$.

^bMeasured in DMF at $-80\text{ }^\circ\text{C}$. ^cThe rate constant for the H_4Q /peroxide reaction at $-80\text{ }^\circ\text{C}$ was obtained by extrapolation from measurements at $+25$ to $-50\text{ }^\circ\text{C}$ using the activation parameters (E_a) obtained from the higher temperature data (see Table S2 in the SI).

spans 1 V with this set of quinone reactants. The free-energy change (ΔG°) of ET from $[\text{K}(18\text{-crown-6})]_2[(\text{O}_2)\text{CmBDCA-5t-H}_6]$ to members of the quinone series is obtained from

$$\Delta G^\circ = -e(E_{\text{red}} - E_1) \quad (6)$$

where $E_1 = -0.85$ V versus $\text{Fc}^{+/0}$ (in DMF) is the reduction potential of $[(\text{O}_2)\text{CmBDCA-5t-H}_6]^{2-}$ and E_{red} is the first reduction potential of the quinones listed in Table 1.^{23,24} The reactions were performed under second-order conditions with identical concentrations of reactants in all cases. The time-resolved diode-array spectra of reactions of the seven quinones and $[\text{K}(18\text{-crown-6})]_2[(\text{O}_2)\text{CmBDCA-5t-H}_6]$ in THF were acquired at -80 °C, except for H_4Q , which required higher temperatures for the reaction to proceed readily (-50 to $+25$ °C). The spectral changes accompanying the ET reaction are shown in Figures 4 and S12–S16 in the SI. To avoid

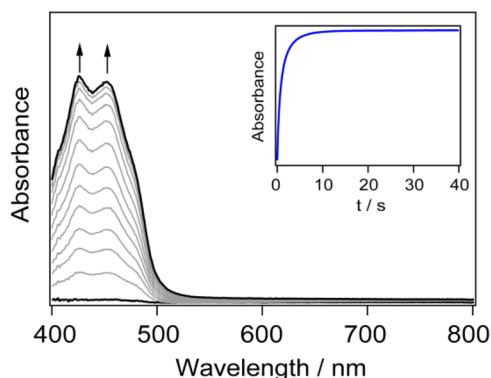


Figure 4. Time-resolved spectral changes obtained upon mixing THF solutions of $[\text{K}(18\text{-crown-6})]_2[(\text{O}_2)\text{CmBDCA-5t-H}_6]$ (0.1 mM) and Cl_2Q (0.1 mM) at -80 °C, showing rapid formation of the $\text{Cl}_2\text{Q}^{\cdot-}$ radical anion. Inset: Kinetic trace at 452 nm acquired in a single-wavelength registration mode. All concentrations are reported after mixing in the stopped-flow cell.

contributions from photochemistry, single-wavelength kinetic traces were acquired at $\lambda = 610$ nm for DDQ, $\lambda = 448$ nm for Cl_4Q and Br_4Q , $\lambda = 432$ nm for F_4Q , $\lambda = 452$ nm for Cl_2Q , $\lambda = 451$ nm for ClQ , and $\lambda = 449$ nm for H_4Q . The kinetic traces in Figures S17–S23 in the SI were analyzed with the bimolecular expression

$$\text{rate} = ae^{-k_{1\text{obs}}t} + be^{-k_{2\text{obs}}t} \quad (7)$$

We note that the kinetic traces for the fastest reactions, $\text{Q} = \text{Cl}_4\text{Q}$ and F_4Q , were not fit well by eq 7. In this case, the traces were better fit by eq 2 to yield $k_{1\text{obs}}$, from which the second-order rate constant was then estimated from $k_{\text{ET}} = k_{1\text{obs}}/[\text{Q}]$. For consistency, kinetic traces from the other four reactions, $\text{Q} = \text{Br}_4\text{Q}$, Cl_2Q , ClQ , and H_4Q , were treated in a similar manner. The rate constant obtained from eq 7 and those estimated from the first-order fitting of the initial segment of the kinetic traces with eq 2 were in accordance with each other.

DISCUSSION

The ability to encapsulate a peroxide dianion within the cage of hexacarboxamide cryptand (*m*BDCA-5t- H_6) permits the ET chemistry of an isolated peroxide ion to be investigated. The homologous quinone series listed in Table 1 allows ET reaction (5) to be analyzed by Marcus theory over a larger driving force. The second-order rate constants listed in Table 1 vary over 6

orders of magnitude, from the mildly endergonic H_4Q system to the most exergonic DDQ system. The driving-force dependence of the ET rate constants is shown in Figure 5,

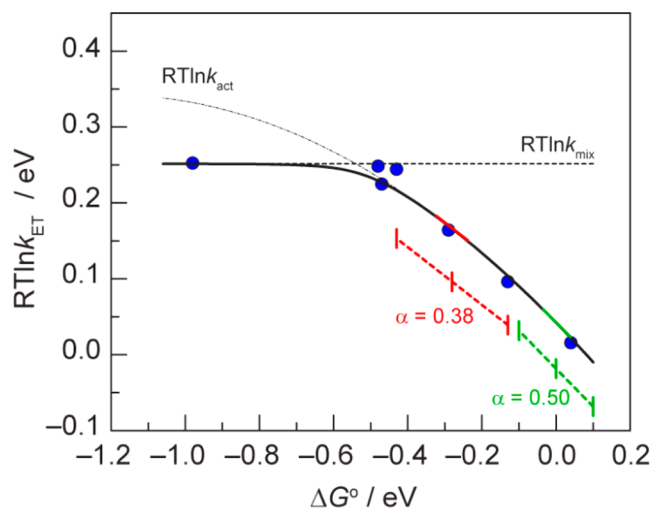


Figure 5. Dependence of $RT \ln k_{\text{ET}}$ on ΔG° for the first one-electron oxidation of $[\text{K}(18\text{-crown-6})]_2[(\text{O}_2)\text{CmBDCA-5t-H}_6]$ with seven different quinones in THF at -80 °C. (black solid line) Marcus curve, eq 11, with $k_{\text{mix}} = 3.8 \times 10^6 \text{ M}^{-1} \text{ s}^{-1}$, $\lambda_{(\text{LO}_2^{\cdot-}/\text{Q})} = 1.2$ eV, and $Z = 9 \times 10^8 \text{ M}^{-1} \text{ s}^{-1}$. The linear regions denoted by $\alpha = 0.38$ (red) and $\alpha = 0.5$ (green) are the tangents of the Marcus curve at the points directly above the midpoints of the lines. Their slopes are -0.38 and -0.5 , respectively.

where the values of $RT \ln k_{\text{ET}}$ are plotted against the driving force (ΔG°). An increase of the $RT \ln k_{\text{ET}}$ values as a function of ΔG° is observed over more than 5 orders of magnitude of k_{ET} in the less exergonic region (-0.48 eV $< \Delta G^\circ < 0.04$ eV). For the strongest oxidant, DDQ (at $\Delta G^\circ = -0.98$ eV), the ET rate appears to level off. However, the ET rate for reaction (1) could not be measured accurately because the mixing time of the stopped-flow instrument has a limiting value, k_{mix} , which we have approximated with $3.8 \times 10^6 \text{ M}^{-1} \text{ s}^{-1}$.

The activation free energy, ΔG^\ddagger , for outer-sphere ET,^{25–27}

$$\Delta G^\ddagger = \frac{(\Delta G^\circ + \lambda)^2}{4\lambda} \quad (8)$$

is related in the Marcus formalism to the free energy of the reaction, ΔG° , and the reorganization energy, λ . In its simplest elaboration, Marcus theory provides the ET rate constant via the Eyring equation

$$k_{\text{act}} = Z \exp\left(-\frac{\Delta G^\ddagger}{RT}\right) \quad (9)$$

where Z is the bimolecular collision frequency, often taken as $\sim 10^{11} \text{ M}^{-1} \text{ s}^{-1}$. In semiclassical expressions of Marcus theory, Z is replaced by nuclear and electronic tunneling terms. In either classical or semiclassical formalisms, by utilizing a series of structurally related quinones, we assume with good confidence that the values for Z and λ are the same for all reactions in the present study. Under this supposition, only changes in ΔG° will influence the magnitude of the measured rate constants.

λ was estimated using the activation energy measured for reaction between ClQ and $[(\text{O}_2)\text{CmBDCA-5t-H}_6]^{2-}$ (Figure S26 in the SI). Assuming that the activation entropy is minimal,

$\Delta G^\ddagger = \Delta H^\ddagger = 24.0$ kJ/mol (0.249 eV), and the reorganization energy for reaction (5) is calculated to be $\lambda_{(\text{LO}_2^{2-}/\text{Q})} = 1.2$ eV. Furthermore, because λ for a cross-reaction is an average of the λ values of the relevant self-exchange reactions,²⁸ the component contributions from the reactant partners $[(\text{O}_2)\text{CmBDCA-5t-H}_6]^{2-}$ and the quinone are furnished from

$$\lambda_{(\text{LO}_2^{2-}/\text{Q})} = \frac{\lambda_{(\text{LO}_2^{2-}/\text{LO}_2^-)} + \lambda_{(\text{Q}/\text{Q}^{\bullet-})}}{2} \quad (10)$$

Values for the self-exchange $\lambda_{(\text{Q}/\text{Q}^{\bullet-})}$ are known to depend on the nature of the counteraction due to ion-pairing effects.²⁹ Though $\lambda_{(\text{Q}/\text{Q}^{\bullet-})}$ has not been measured with K(18-crown-6)⁺ as the cation, it has been measured for quinones with counteractions of K([2,2,2]cryptand)⁺, $\lambda_{(\text{Q}/\text{Q}^{\bullet-})} = 0.42$ eV, and K(THF)₄⁺, $\lambda_{(\text{Q}/\text{Q}^{\bullet-})} = 0.99$ eV.²⁹ Taking an average of these two values to approximate $\lambda_{(\text{Q}/\text{Q}^{\bullet-})} = 0.71$ eV for K(18-crown-6)⁺, then the estimate of $\lambda_{(\text{LO}_2^{2-}/\text{LO}_2^-)} = 1.7$ eV is determined from eq 10.

For the stopped-flow experiment, the observed ET rate constant is convoluted with the mixing time of the reactants. The equation that governs the observable ET kinetics is

$$\frac{1}{k_{\text{ET}}} = \frac{1}{k_{\text{mix}}} + \frac{1}{k_{\text{act}}} = \frac{1}{k_{\text{mix}}} + \frac{1}{Z \exp\left[\frac{-(\Delta G^\circ + \lambda)^2}{4\lambda RT}\right]} \quad (11)$$

This equation is a double-reciprocal model for the observable kinetics in a stopped-flow instrument, which has an inherent mixing time defined by k_{mix} .³⁰ Using $\lambda_{(\text{LO}_2^{2-}/\text{Q})} = 1.2$ eV, which was deduced from the temperature dependence of the reaction with ClQ and the driving force for the ET reactions, the observed measurements are approximated by eq 11 for $Z = 9 \times 10^8$ M⁻¹ s⁻¹ (Figure 5). Figure S26 in the SI shows a comparison of the plots derived from eq 11 for a range of Z values.

The differentiated Marcus expression yields

$$\begin{aligned} \frac{\partial RT \ln k_{\text{ET}}}{\partial \Delta G^\circ} &= \frac{\partial}{\partial \Delta G^\circ} \left[RT \ln Z - \left(\frac{\lambda}{4} + \frac{\Delta G^\circ}{2} + \frac{\Delta G^{\circ 2}}{4\lambda} \right) \right] \\ &= -\frac{1}{2} \left(1 + \frac{\Delta G^\circ}{\lambda} \right) \end{aligned} \quad (12)$$

This equation defines the local slope in the activation controlled regime of the curve in Figure 5 at any driving-force value. For the driving-force range of $\lambda \gg |\Delta G^\circ|$, as depicted in the green region in Figure 5, a linear free-energy relationship (LFER) is obtained with a slope -0.5 . For a regime in which the average driving force is $1/4$ the magnitude of λ , as depicted by the red region of Figure 5, then a LFER is obtained with a slope of -0.38 . In this study, the specific quinones were chosen such that a large range of driving force was explored and, therefore, we prefer to model the Marcus kinetics with the quadratic Marcus equation (eq 11), as shown by the black solid line in Figure 5. The data in the activation control region fit this expected curve, with a limiting region eventually achieved because of the mixing time of the stopped-flow spectrometer.

The homogeneous ET kinetics of LO_2^{2-} , as explained by Figure 5, is related to its heterogeneous ET reaction at an electrode surface, as defined by the CVs of Figure 2. The Butler–Volmer model of electrode kinetics accounts for a rate-limiting ET and is characterized by the symmetry factor, α , also known as the transfer coefficient. This transfer coefficient is the

linchpin between the Butler–Volmer model and the Marcus ET formalism.^{31,32} Formally, the transfer coefficient is defined as

$$\alpha = \frac{\partial \Delta G^\ddagger}{\partial \Delta G^\circ} \quad (13)$$

Within the context of Butler–Volmer kinetics, it is assumed, without any theoretical basis, that a linear relationship exists between ΔG^\ddagger and ΔG° . In Marcus theory, ΔG^\ddagger has a quadratic dependence on ΔG° , according to eq 8, leading to

$$\alpha = \frac{1}{2} \left(1 + \frac{\Delta G^\circ}{\lambda} \right) \quad (14)$$

Excursions in the potential around the standard reduction potential involving small molecules are typically small, in the range of 30–200 mV, and thus $\lambda \gg |\Delta G^\circ|$. Therefore, in most electrochemical experiments, the transfer coefficient is in the linear Marcus regime where $\alpha = 0.5$ (green region of Figure 5) and a Butler–Volmer approximation with $\alpha = 0.5$ is often appropriate. However, when the electrode kinetics is sluggish owing to poor coupling to the electrode, large driving-force overpotentials are required to produce a peak current response in a CV, despite moderate or low values of λ . Therefore, according to eq 14, as the absolute magnitude of ΔG° approaches λ , the value of the transfer coefficient will decrease from $\alpha = 0.5$ to a lower value, depending precisely on the ratio of $\Delta G^\circ/\lambda$. In a graphical sense, the measured current response is then occurring in a region of the Marcus curve that is closer to the curve's apex, for example, in the red region of Figure 5.

The electrode kinetics of $[\text{TBA}]_2[(\text{O}_2)\text{-CmBDCA-5t-H}_6]$ is consistent with this latter case. Simulation of the CVs of $[(\text{O}_2)\text{CmBDCA-5t-H}_6]^{2-}$ yields a heterogeneous ET rate constant of $k_s = 2.7 \times 10^{-5}$ cm/s, which places ET on the border of what is commonly accepted as an electrochemically quasi-irreversible or irreversible ET.³³ The broadness of the wave is in accordance with the attenuated transfer coefficient of $\alpha = 0.38$, as determined from the Butler–Volmer model.¹¹ By modeling the CV features using the Marcus–Hush model of electrokinetics, λ may be obtained, where α is treated as a variable according to eq 14.³⁴ We find a heterogeneous reorganization energy of $\lambda_{\text{el}} = 0.79$ eV from the electrochemical simulations (vide supra). This electrochemical-derived reorganization energy can be compared to the homogeneous reorganization energy derived from the fit of the Marcus curve in Figure 5, though not directly. The homogeneous reorganization energy, $\lambda_{(\text{LO}_2^{2-}/\text{LO}_2^-)}$, is defined for a bimolecular self-exchange reaction, which includes contributions from two reactant molecules, whereas the electrochemical reorganization energy involves only a single-molecule reactant (there is no contribution from the electrode surface). Therefore, the correct comparison is between the electrochemical reorganization energy, λ_{el} , and $1/2\lambda_{(\text{LO}_2^{2-}/\text{LO}_2^-)}$,³⁵

$$\frac{1}{2}\lambda_{(\text{LO}_2^{2-}/\text{LO}_2^-)} = 0.85 \text{ eV} \quad (15)$$

The agreement between the two reorganization energies is quite good considering that the assumption of an intermediate reorganization energy for quinones in the presence of the cation, K(18-crown-6)⁺, was needed to arrive at the homogeneous reorganization energy for $[(\text{O}_2)\text{CmBDCA-5t-H}_6]^{2-}$ oxidation (vide supra).

With the heterogeneous rate constant, k_s , and reorganization energy, a heterogeneous preexponential factor, Z_{el} , can also be derived using eq 9 with $\Delta G^\ddagger = \lambda_{el}/4$. We find $Z_{el} = 0.059$ cm/s, which is 5 orders of magnitude lower than the collision frequency $Z_{el} = (RT/2\pi M)^{1/2} = 2000$ cm/s, where M is the molar mass of $[(O_2)CmBDCA-5t-H_6]^{2-}$. This disparity is consistent with the results of homogeneous ET, in which a preexponential factor of $Z = 9 \times 10^8$ M⁻¹ s⁻¹ was found to be 2 orders of magnitude lower than the classical value. The diminished preexponential factor, whether ET by LO_2^{2-} occurs to a molecule or electrode, is attributed to poor electronic coupling³⁶ because of steric shielding of O_2^{2-} within the hexacarboxamide cryptand. Because the electron acceptor in the homogeneous reaction, the quinone, is small and may have partial access to the cavities presented by the cryptand molecule, whereas the heterogeneous electron acceptor, the electrode, does not, it is not surprising that the heterogeneous ET event exhibits even greater nonadiabatic character than the homogeneous ET.

CONCLUSIONS

A free peroxide ion may be isolated within the cage of a hexacarboxamide cryptand, thus allowing for the ET reactivity of this dianion of oxygen to be examined. Enhanced solubility of $[(O_2)CmBDCA-5t-H_6]^{2-}$ in THF is enabled by sequestration of the K^+ counterions by 18-crown-6, thus allowing for the study of homogeneous ET via the stopped-flow method. The ET reaction of the encapsulated peroxide with quinones is consistent with a highly nonadiabatic outer-sphere transfer owing to steric shielding of peroxide from its reacting partner by the hexacarboxamide cryptand. These results correlate well with the heterogeneous ET rate measurements, which exhibit an apparent transfer coefficient of $\alpha < 0.5$. Modeling the $[(O_2)CmBDCA-5t-H_6]^{2-}$ electrochemical response within a Marcus theory framework yields a consistent set of results for the homogeneous and heterogeneous ET reactions. We have emphasized in this study the direct relationship between the local slope of the Marcus curve and α . For nonadiabatic ET, α can be treated as a variable that depends on the driving force. The λ value thus obtained is consistent with that obtained in homogeneous Marcus analysis. This is one of the few cases^{37,38} where a direct comparison between homogeneous and heterogeneous ET reactions for a given species has been made. Understanding the intrinsic parameters that govern the kinetics of ET from this unique species will facilitate its development as a reagent for oxidations, reductions, and/or atom-transfer chemistries.

The most fundamental reaction of all molecular oxygen species is ET. Owing to our success in using a macro-bicyclic anion receptor³⁹ to furnish an isolated peroxide dianion species that is soluble in aprotic organic media, the kinetics of the transfer of an electron from the peroxide dianion in the absence of an intimately bound proton or metal ion has now been established. Considering the importance of peroxide as an intermediate in biochemical redox processes, as a valuable industrial feedstock, and as a primary discharge product in nonaqueous lithium–air batteries, the results reported herein provide a basis for elucidating the chemistry of peroxide in a range of subjects pertaining to oxygen and ET.

ASSOCIATED CONTENT

Supporting Information

X-ray crystallographic data in CIF format, CVs, parameters used for simulation of CVs, stopped-flow kinetic traces, decay kinetics and summary of stopped-flow data, ¹H NMR spectra, electrochemical plots of the potential and current versus scan rate, kinetic traces for the formation of quinone anions, time-resolved stopped-flow spectral changes accompanying ET between LO_2^{2-} and quinones, Cl_4Q , F_4Q , Br_4Q , ClQ , and H_4Q . Arrhenius and Eyring plots, and Marcus curve plots with different Z factors. This material is available free of charge via the Internet at <http://pubs.acs.org>. Complete crystallographic data were deposited in the Cambridge Crystallographic Database Centre (CCDC 983504).

AUTHOR INFORMATION

Corresponding Authors

*E-mail: ccummins@mit.edu.

*E-mail: dnocera@fas.harvard.edu.

Funding

D.G.N. acknowledges support of the Department of Energy (DOE; Grant DE-SC0009758). C.C.C. acknowledges support of the NSF-CCI (Grant CHE-0802907). E.V.R.-A. acknowledges support of the DOE (Grant DE-FG02-06ER15799). Grants from the NSF also provided instrument support to the DCIF at MIT (Grants CHE-9808061 and DBI-9729592) and to E.V.R.-A. at Tufts (Grants CRIF CHE-0639138 and MRI CHE-1229426). D.J.G. acknowledges the support of the NSF's Graduate Research Fellowship Program. The authors also acknowledge the Robert Bosch Company for partial financial support.

Notes

The authors declare no competing financial interest.

REFERENCES

- (1) Sawyer, D. T. *Oxygen Chemistry*; Oxford University Press: New York, 1991.
- (2) Sawyer, D. T.; Valentine, J. S. *Acc. Chem. Res.* **1981**, *14*, 393–400.
- (3) Sawyer, D. T.; Chiericato, G.; Angelis, C. T.; Nanni, E. J.; Tsuchiya, T. *Anal. Chem.* **1982**, *54*, 1720–1724.
- (4) Stanbury, D. M.; Mulac, W. A.; Sullivan, J. C.; Taube, H. *Inorg. Chem.* **1980**, *19*, 3735–3740.
- (5) Costentin, C.; Evans, D. H.; Robert, M.; Savéant, J.-M.; Singh, P. S. *J. Am. Chem. Soc.* **2005**, *127*, 12490–12491.
- (6) Goolsby, A. D.; Sawyer, D. T. *Anal. Chem.* **1968**, *40*, 83–86.
- (7) Imlay, J. A. *Annu. Rev. Biochem.* **2008**, *77*, 755–776.
- (8) Jones, C. W. *Applications of Hydrogen Peroxide and Derivatives*; Royal Society of Chemistry: Cambridge, U.K., 1999.
- (9) Huff, L. A.; Rapp, J. L.; Zhu, L.; Gewirth, A. A. *J. Power Sources* **2013**, *235*, 87–94.
- (10) Abraham, K. M.; Jiang, Z. *J. Electrochem. Soc.* **1996**, *143*, 1–5.
- (11) Lopez, N.; Graham, D. J.; McGuire, R.; Alliger, G. E.; Shao-Horn, Y.; Cummins, C. C.; Nocera, D. G. *Science* **2012**, *335*, 450–453.
- (12) Chen, Y.; Freunberger, S. A.; Peng, Z.; Fontaine, O.; Bruce, P. G. *Nat. Chem.* **2013**, *5*, 489–494.
- (13) McCloskey, B. D.; Scheffler, R.; Speidel, A.; Girishkumar, G.; Luntz, A. C. *J. Phys. Chem. C* **2012**, *116*, 23897–23905.
- (14) Lu, Y.-C.; Gallant, B. M.; Kwabi, D. G.; Harding, J. R.; Mitchell, R. R.; Whittingham, M. S.; Shao-Horn, Y. *Energy Environ. Sci.* **2013**, *6*, 750–768.
- (15) Christensen, J.; Albertus, P.; Sanchez-Carrera, R. S.; Lohmann, T.; Kozinsky, B.; Liedtke, R.; Ahmed, J.; Kojic, A. *J. Electrochem. Soc.* **2012**, *159*, R1–R30.
- (16) Sheldrick, G. M. *Acta Crystallogr., Sect. A* **2008**, *64*, 112–122.
- (17) Müller, P. *Crystallogr. Rev.* **2009**, *15*, 57–83.

- (18) Wilshire, J.; Sawyer, D. T. *Acc. Chem. Res.* **1979**, *12*, 105–110.
- (19) Ortiz, M. E.; Nuñez-Vergara, L. J.; Squella, J. A. *J. Electroanal. Chem.* **2003**, *549*, 157–160.
- (20) Savéant, J.-M. *Elements of Molecular and Biomolecular Electrochemistry*; John Wiley: Hoboken, NJ, 2006; p 105.
- (21) Rudolf, M. *J. Electroanal. Chem.* **2003**, *543*, 23–39. DigiElch from Elchsoft under <http://www.elchsoft.com>.
- (22) Miller, J. S.; Krusic, P. J.; Dixon, D. A.; Reiff, W. M.; Zhang, J. H.; Anderson, E. C.; Epstein, A. J. *J. Am. Chem. Soc.* **1986**, *108*, 4459–4466.
- (23) Ebersson, L. *Acta Chem. Scand.* **1999**, *53*, 584–593.
- (24) Peover, M. E. *J. Chem. Soc.* **1962**, 4540–4548.
- (25) Marcus, R. A. *Annu. Rev. Phys. Chem.* **1964**, *15*, 155–196.
- (26) Marcus, R. A. *Angew. Chem., Int. Ed.* **1993**, *32*, 1111–1121.
- (27) Marcus, R. A.; Sutin, N. *Biochim. Biophys. Acta* **1985**, *811*, 265–322.
- (28) Sutin, N. In *Inorganic Reaction and Methods*; Zuckerman, J. J., Ed.; Wiley-VCH: Weinheim, Germany, 1986; Vol. 15, pp 41–45.
- (29) Lu, J.-M.; Rosokha, S. V.; Neretin, I. S.; Kochi, J. K. *J. Am. Chem. Soc.* **2006**, *128*, 16708–16719.
- (30) Nemeth, M. T.; Fogelman, K. D.; Ridley, T. Y.; Margerum, D. *W. Anal. Chem.* **1987**, *59*, 283–291.
- (31) Bard, A.; Faulkner, L. R. *Electrochemical Methods: Fundamentals and Applications*, 2nd ed.; John Wiley: Hoboken, NJ, 2001; pp 121–124.
- (32) Savéant, J.-M. *Elements of Molecular and Biomolecular Electrochemistry*; John Wiley: Hoboken, NJ, 2006; pp 30–44.
- (33) Geiger, W. E. In *Inorganic Reaction and Methods*, Zuckerman, J. J., Ed.; Wiley-VCH: Weinheim, Germany, 1986; Vol. 15, pp 88–91.
- (34) Feldberg, S. W. *Anal. Chem.* **2010**, *82*, 5176–5183.
- (35) Weaver, M. J. In *Inorganic Reaction and Methods*; Zuckerman, J. J., Ed.; Wiley-VCH: Weinheim, Germany, 1986; Vol. 15, pp 153–163.
- (36) Costentin, C. *Chem. Rev.* **2008**, *108*, 2145–2179.
- (37) Kojima, H.; Bard, A. J. *J. Am. Chem. Soc.* **1975**, *97*, 6317–6324.
- (38) Costentin, C.; Hajj, V.; Louault, C.; Robert, M.; Savéant, J.-M. *J. Am. Chem. Soc.* **2011**, *133*, 19160–19167.
- (39) Sessler, J. L.; Gale, P. A.; Cho, W.-S. *Anion Receptor Chemistry*; Royal Society of Chemistry: Cambridge, U.K., 2006.